Journal of Cardiology 73 (2019) 544–552

Contents lists available at ScienceDirect

Journal of Cardiology

journal homepage: www.elsevier.com/locate/jjcc

Original article

Patient-specific non-invasive estimation of pressure gradient across aortic coarctation using magnetic resonance imaging

Yubing Shi (PhD)[a,1], Israel Valverde (MD)[b,c], Patricia V. Lawford (PhD)[a], Philipp Beerbaum (MD)[b], D. Rodney Hose (PhD)[a,*]

[a] Medical Physics Group, Department of Cardiovascular Science, Faculty of Medicine, Dentistry and Health, University of Sheffield, Sheffield, UK
[b] Division of Imaging Sciences and Biomedical Engineering, King's College London, The Rayne Institute, St. Thomas' Hospital, London, UK
[c] Cardiovascular Pathology Unit, Institute of Biomedicine of Seville (IBIS), CIBER-CV, Hospital Virgen de Rocio/CSIC/University of Seville, Seville, Spain

ARTICLE INFO

Article history:
Received 10 April 2018
Received in revised form 5 November 2018
Accepted 11 December 2018
Available online 29 January 2019

Keywords:
Pressure gradient
Aortic coarctation
Magnetic resonance imaging
Model prediction
Bernoulli equation
Inertial effect

ABSTRACT

Background: Non-invasive estimation of the pressure gradient in aortic coarctation has much clinical importance in assisting the diagnosis and treatment of the disease. Previous researchers applied computational fluid dynamics for the prediction of the pressure gradient in aortic coarctation. The accuracy of the prediction was satisfactory but the procedure was time-consuming and resource-demanding.
Method: In this research a magnetic resonance imaging (MRI)-based non-invasive modeling procedure is implemented to predict the pressure gradient in 14 patient cases of aortic coarctation. Multi-cycle patient flow and pressure data are processed to produce the flow and pressure conditions in the patient cases. Bernoulli equation-based friction loss model combined with the inertial effect of the blood flow in the vessel segments are applied to model the pressure gradient in the aortic coarctation. The model-predicted pressure gradient data are then compared with the catheter in vivo measurement data for validation.
Results: The MRI-based model prediction technique produces results that are consistent with those from the catheter measurement, based on the criteria of both the cycle-averaged instantaneous pressure gradient and the peak-to-peak pressure gradient.
Conclusion: This study suggests that the MRI-based non-invasive modeling procedure has much potential to be applied in clinical practice for the prediction of the pressure gradient in aortic coarctation patients.

Introduction

Aortic coarctation (AoCo) is a narrowing in the descending thoracic aorta distal to the origin of the left subclavian artery and in the region of the ductus arteriosus. It may be represented either as a localized stenosis or as a hypoplastic segment [1]. Without treatment it causes long-term complications such as systemic hypertension, accelerated coronary heart disease, stroke, aortic dissection, and congestive heart failure [2]. Clinical investigation of AoCo often requires imaging and invasive catheter measurements of the pressure gradient across the coarctation, and surgical interventions are indicated when the pressure gradient under rest condition is greater than 20 mmHg [3].

Although the catheterization technique for the purpose of invasive hemodynamic monitoring and cardiovascular treatment has been routinely used in clinical practice, it is nevertheless a procedure susceptible to complications of thrombus formation, thromboembolism, bacterial colonization and septicemia, blood/air embolism, and ischemic damage [4,5]. For this reason, a non-invasive approach as the alternative technique for the hemodynamic monitoring is highly desirable.

In the past decades, a number of computational fluid dynamics (CFD) modeling studies have been conducted to give non-invasive predictions of the pressure gradient in the AoCo [6–9]. These studies suggest that CFD models gave accurate prediction of the

* Corresponding author at: Medical Physics Group, Department of Cardiovascular Science, Faculty of Medicine, Dentistry and Health, University of Sheffield, Sheffield, S10 2RX, UK.
E-mail address: d.r.hose@sheffield.ac.uk (D.R. Hose).
[1] Present address: Faculty of Arts, Science, and Technology, University of Northampton, Northampton, UK.

https://doi.org/10.1016/j.jjcc.2018.12.016
0914-5087/

pressure gradient in the AoCo, as long as the boundary conditions were set realistically based on the clinically measured data. However, such analysis is always time-consuming, with the typical computing time in the range of 6–145 h on a workstation class multi-processor computer depending on the choice of the accuracy level [6]. Such a huge computing time makes CFD a suitable research tool but not a proper clinical analysis tool.

In the past, researchers have been using a series of simplified equations, either empirical or derived from fluid mechanics theory, for the non-invasive clinical estimation of the pressure gradient in cardiovascular stenosis (including in heart valves, atherosclerosis, and AoCo). In these simplified models, flow velocity and the geometry of the flow channel in the stenosis were estimated from either Doppler echocardiography [10–20] or magnetic resonance imaging (MRI) [21–23] measurements. This non-invasive procedure seemed to achieve fair agreement in the diagnosis of stenosis in heart valves and atherosclerosis, and has been extended to analyze other vascular diseases [24,25]. However, its application to the AoCo situation is rare in the literature.

This paper describes a MRI-based non-invasive prediction of the pressure gradient in 14 AoCo patient cases, and the model predicted data are compared with those measured through cardiac catheterization for validation. This helps us to judge whether the non-invasive model prediction can be used to produce a cost-effective clinical diagnosis of the pressure gradient in the AoCo.

Methods

In this research, we are analyzing 14 cases of MRI-measured patient data for the study of non-invasive estimation of the pressure-gradient in the AoCo condition. The patient vessel geometries and flow are measured with MRI. Simple lumped-parameter models are constructed to describe the combined frictional loss and blood inertia effect in estimating the pressure gradient in each patient case. The estimated pressure gradients are then compared with the catheter-measured pressure gradient for validation.

Patient selection

The study population includes 14 cases with AoCo (age 21 ± 7 years, weight 71 ± 16 kg) (Table 1). The patients had different degrees of AoCo condition as described by the coarctation index (COI), which is defined as the ratio of the aortic sectional area for the stenosed section over the unstenosed aorta at the level of the diaphragm. The research was performed at St. Thomas' Hospital between June 2007 and June 2011. The local research ethic committee approved this prospective study, and informed consent was obtained from all patients (Ethics reference number R&D REC 08/H0804/134). Inclusion criteria comprise native or residual AoCo. Exclusion criteria were the presence of stented AoCo or aortic dissection.

Magnetic resonance imaging and in vivo pressure/flow measurements

The clinical data acquisition is performed in a hybrid magnetic resonance (MR)/X-ray suite (XMR) guidance system [integration of a 1.5-T cylindrical bore MR scanner (Philips Intera I/T, Philips, Amsterdam, the Netherlands) using a 5-element channel cardiac surface coil and a mobile cardiac X-ray set (Philips BV Pulsera)]. The combined X-ray cardiac catheterization and MRI investigations are performed as described by Muthurangu et al. [26]: patients had general anesthesia according to institutional protocol. Fiducial markers are put on the skin to allow X-ray and MRI image registration [27]. Two femoral artery vascular accesses by percutaneous puncture are obtained (5-6F sheath) and heparin is administered (50 IE/kg). Under fluoroscopy guidance, a multi-purpose catheter (angiographic catheter 4F with carbon dioxide-filled balloon) is advanced from the right femoral artery to the ascending aorta just above the aortic sinus. A second multi-purpose catheter in the left femoral artery is advanced to the abdominal aorta at the level of the diaphragm. The floating table is then moved to transfer the patient to the MRI scan.

The MRI protocol includes a breath-hold 3D-contrast enhanced angiography to image the aorta (sagittal orientation, field of view 260–350 mm × 240–280 mm in foot-head and anterior–posterior direction respectively, slice thickness 1.5 mm, 90–120 slices, matrix 240–280 mm × 240–280 mm, acquired voxel size 1.5 mm × 1.5 mm × 1.5 mm, reconstructed voxel size 1.5 mm × 1.5 mm × 1.5 mm, fold-over direction anterior-posterior, repetition time/echo time 4.4 ms/1.3 ms, flip angle 40°, SENSE factor 1.6, temporal phase 2, time-delay between phases 10–15 s, dynamic scan time 25–30 s per dynamic scan, total scan duration 100–120 s, number of signal averages 1). The gadolinium-based contrast agent is injected intravenously by hand at a dose of 0.2 mmol/kg (Magnevist, Berlex Laboratories, Hanover, NJ, USA). The preferred injection site was the right or left antecubital vein. We used a real-time bolus track (coronal slice, thickness 120 mm, located at the level of the heart and superior vena cava) to visualize the bolus injection. The acquisition and breath-hold were simultaneously triggered when contrast was seen arriving at the right atrium-right ventricle. The first dynamic scan usually showed

Table 1
Patient statistics.

Case no.	Age	M/F	Weight (kg)	HR (bpm)	COI	CO (L/min)	Peak, P_{asc} (mmHg)	Peak, P_{dsc} (mmHg)	ΔP (mmHg)
1	17	M	71	47	0.8	3.70	82.09	72.95	9.14
2	35	M	95	61	0.74	5.98	95.57	79.84	15.73
3	12	M	46	77	0.49	3.47	120.12	99.86	20.26
4	35	M	63	55	1.17	6.40	100.97	100.92	0.05
5	18	M	72	60	1.07	5.79	86.84	76.82	10.02
6	25	M	92	46	0.55	3.92	100.36	101.42	-1.06
7	16	F	52	60	0.85	3.91	91.49	69.97	21.52
8	15	M	59	48	0.41	2.90	100.78	79.92	20.86
9	25	M	64	86	0.67	5.20	81.88	64.55	17.33
10	21	M	95	69	0.93	4.52	79.1	70.77	8.33
11	20	M	71	81	0.63	4.78	79.76	71.57	8.19
12	15	F	88	80	0.83	4.82	85.93	76.36	9.57
13	18	M	64	51	0.74	3.86	92.66	88.38	4.28
14	20	M	63	71	0.81	5.48	79.15	78.99	0.16
Mean:	21 ± 7		71 ± 16	71 ± 16	0.76 ± 0.21	4.62 ± 1.05	91.19 ± 11.66	80.00 ± 12.15	10.31 ± 7.84

Note: HR, heart rate; COI, coarctation index; CO, cardiac output; ΔP, pressure gradient.

the right ventricle and pulmonary arteries. The aorta was usually better seen at the second dynamic scan. From the multiple 3D steady-state slices triggered to the electrocardiogram (imaging was acquired in a sagittal orientation, field of view 280–350 mm × 250–280 mm in foot-head and anterior-posterior direction respectively, number of slices 100–120; isotropic resolution, 1.5 mm × 1.5 mm × 1.5 mm; repetition time/echo time, 3.4 ms/1.7 ms; flip angle, 90°; acquisition window, 60–75 ms, usually triggered at mid-systole and late diastole) [28], the one for systole is chosen based on quantifying the volume of the aortic lumen. The raw flow data are extracted at equally spaced time steps with an independent diagnostic workstation (View Forum, Philips). The flow velocity information at rest is obtained by free-breathing 2D-phase contrast flow through-plane at the level of the ascending and upper descending aorta [field of view 300 mm × 350 mm, matrix 176 × 176, acquired voxel size 1.7 mm/1.7 mm, reconstructed voxel size 1.2 mm × 1.2 mm, slice thickness 7 mm, repetition time/echo time 4.7 ms/3.1 ms, flip angle 15°, velocity encoded value set to 3.5 ms, temporal phases 80–100 per cardiac cycle, 2 numbers of excitation, SENSE 1.7, phase-coding direction anterior-posterior, duration (depending on heart rate) usually between 1.0 min and 2.5 min].

Additionally, 2D-flow sequence at the level of the supra-aortic branches is acquired using the same sequence as above, but with the velocity encoded value set to 2.0 m/s. Just after the flow acquisition, a 15–20 s breath-hold is performed to simultaneously register the catheter pressures in the ascending and diaphragmatic aorta with a 1 kHz sampling rate. This effectively avoids the complications during the recording associated with the contact condition between the catheter tip and the vessel wall. We found that pressure tracing recordings were more accurate and with less motion artifacts during breath-hold, with no significant change in overall systolic and diastolic pressure recording.

Processing of in vivo measured pressure and flow data

Phase contrast MRI measurement provides the cycle-averaged flow variation at the aortic root and the diaphragm positions in a complete heart cycle. Pressures in the aortic root and the diaphragm positions are measured separately from the MRI flow data, using X-ray cardiac catheterization. The pressures are measured at a 1 kHz sampling rate over 20–50 heart cycles. The cycle data sequence are then divided into different heart cycles based on the main features of the maximum and the minimum values in the heart cycles. A statistical analysis is then applied to the cycle divided data, to find the mean values and the standard errors of several cardiac indexes including the peak systolic pressure, trough diastolic pressure, heart period, peak pressure rising time (time from the start of the heart cycle to the instance corresponding to the peak systolic pressure). Those cycles with any one of the above indexes deviated too much are rejected. The mean value of the heart periods T in the selected cycles is then chosen as the reference heart period, and a representative data cycle for the ascending/descending pressure is constructed by interpolation from and average-processing of those selected cycles. The ascending and descending aortic pressures are recorded in the same procedure so they have the same heart period, but the pressure and flow data were measured at different times and using different techniques, so the heart periods between the pressure and flow are not precisely equal. To keep the consistency among the data, the processed pressure data are then normalized using the cycle period of the corresponding aortic root flow in the individual patient case.

To evaluate the difference between the model-predicted pressure gradient and the in vivo measured pressure gradient in the AoCo in the patient cases, two index variables are defined in the study and used in the processing of the results data. These are the mean prediction error, defined as:

$$(\Delta(\Delta P)) = \frac{1}{T}\int_0^T dP_{model}(t) - [P_{asc}(t) - P_{dsc}(t)dt,$$

and the root mean square (RMS) of the model prediction error, defined as:

$$(\Delta(\Delta P)) = \sqrt{\frac{1}{T}\int_0^T dP_{model}(t) - [P_{asc}(t) - P_{dsc}(t)^2 dt}.$$

In the equations, P_{asc} is the in vivo measured ascending aortic pressure; P_{dsc} the in vivo measured descending aortic pressure; and dP_{model} is the model predicted pressure gradient across the AoCo.

Simplified blood flow model to assist estimation of the pressure gradient

Blood flow response in the aorta is mainly influenced by the factors of frictional loss, blood inertia, and the vessel wall elasticity. As the vessel wall elasticity is difficult to quantify through cardiac imaging, the current study chooses to neglect the wall elasticity and then observe how much the difference in the pressure gradient results is accompanying such a simplification. The frictional loss is not remarkable in the healthy aorta, but it becomes the major contributor to the overall pressure gradient in the cardiovascular stenosis as in the AoCo. Previous researchers have developed a series of simplified equations to calculate the pressure gradient in the cardiovascular stenosis. Among these, the Bernoulli's equation with full kinetic loss as summarized by Weyman and Scherrer-Crosbie [29] is adopted in this study, because it maintains a balance between simplicity and accuracy. The equation can be represented as:

$$\Delta P_{friction} = P_u - P_d \approx P_u - P_s = \frac{\rho}{2}({v_s}^2 - {v_u}^2) = \frac{\rho Q^2}{2}\left(\frac{1}{{A_s}^2} - \frac{1}{{A_u}^2}\right). \quad (1)$$

In Eq. (1), $\Delta P_{friction}$ is the pressure drop due to the frictional effect; P_u the pressure at the upstream side/proximal side of the stenosis; P_d the pressure at the downstream side/distal side of the stenosis; P_s the pressure at the narrowest section of the stenosis; ρ the density of the blood; Q the flow rate; v_u and v_s the velocities at the proximal side of the stenosis and at the narrowest section of the stenosis; A_u and A_s are the sectional areas of the flow channels at the proximal side of the stenosis and at the narrowest section of the stenosis.

The effect of blood inertia is decided by the rate of flow changes as well as the length and sectional area of the vessel segment involved. When the pressure gradient was evaluated between the immediate upstream and downstream vessel planes or under the steady flow condition, the effect of blood inertia is relatively minor and can be neglected without causing much difference in results. However, in the clinical catheter measurement of the pressure gradient in the AoCo, the measurement positions are usually far upstream and downstream of the vessel stenosis (for example, the proximal measurement location is often in the aortic root, which can be 0.03–0.06 m upstream of the coarctation; and the distal measurement position is often in the diaphragm aorta position or even near iliac artery, which can be 0.15–0.5 m downstream of the coarctation), and the blood flow is pulsatile in the aorta, thus the blood inertia becomes another important contributor to the overall pressure gradient. The inertia effect in the aortic flow can be

described by the simplified relation of:

$$\frac{dv}{dt} = \frac{1dP}{\rho dx}, \tag{2}$$

where v is the flow velocity and x is the axial location.

Multiply the vessel sectional area to both sides of the above equation, and there is:

$$A\frac{dv}{dt} = \frac{dQ}{dt}A\frac{dp}{dx} \approx \frac{\Delta P}{(\rho \cdot \Delta x)/A} = \frac{\Delta P}{L}. \tag{3}$$

where the blood inertia effect $L = (\rho \cdot \Delta x)/A$ is a function of the blood density, length of the vessel segment, and the sectional area of the vessel. Thus the pressure drop due to the inertial effect ($\Delta P_{inertia}$) is:

$$\Delta P_{inertia} = L \cdot \frac{dQ}{dt}. \tag{4}$$

The overall pressure gradient ΔP_{all} is a summation of the pressure loss due to the blood inertia and due to the frictional loss:

$$\Delta P_{all} = \Delta P_{inertia} + \Delta P_{friction} = L \cdot \frac{dQ}{dt} + \frac{\rho Q^2}{2}\left(\frac{1}{\frac{2}{s}} - \frac{1}{A_u^2}\right). \tag{5}$$

The geometrical configuration of the stenosis in the individual AoCo patient changes from person to person, thus Eq. (5) needs to be adapted to suit the individual situations as necessary. For example, Fig. 1a shows the equivalent circuit representation of a simple vessel configuration, while Fig. 1b illustrates another more complex one in which the contribution of each vessel segment is modeled individually. For the AoCo situation as described in Fig. 1a, the blood flow model is represented with:

$$\Delta P_{all} = L_{asc} \cdot \frac{dQ_{asc}}{dt} + L_{dsc} \cdot \frac{dQ_{dsc}}{dt} + \frac{\rho Q_{dsc}^2}{2}\left(\frac{1}{A_s^2} - \frac{1}{A_u^2}\right). \tag{6a}$$

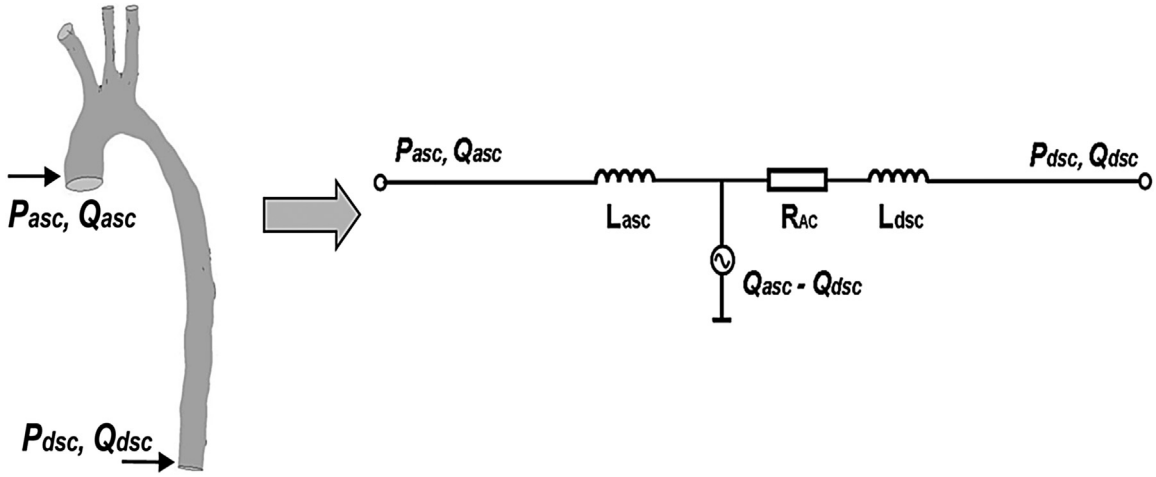

(a) A simple vessel configuration

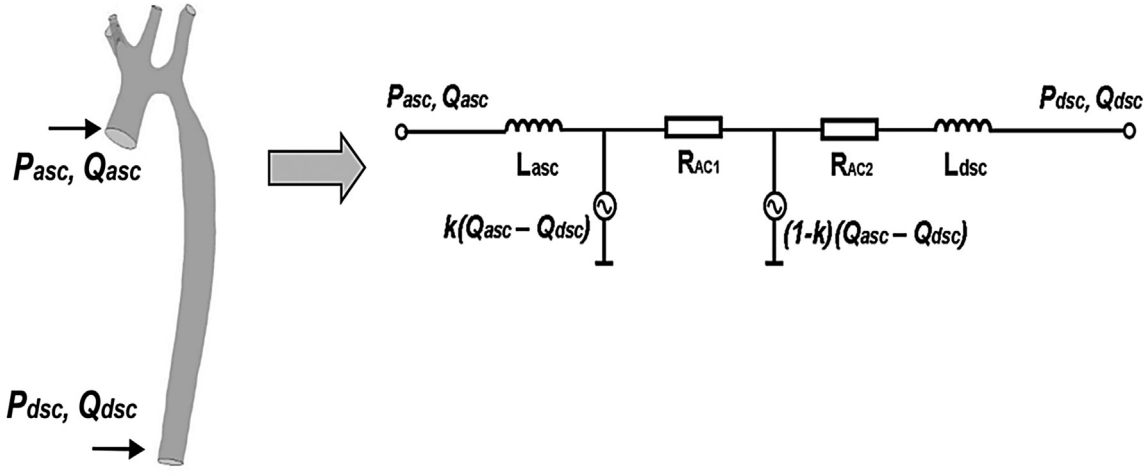

(b) A more complex vessel configuration

Fig. 1. Lumped-parameter blood flow models in the aorta with aortic coarctation. (*Note*: *P*, pressure; *Q*, flow rate; *R*, frictional effect in the blood flow; *L*, inertial effect of the blood flow. R_{AC} describes the frictional effect in the aortic coarctation.)

Table 2
Configuration of the lumped-parameter blood flow model used for each patient case.

Case no.	Model configuration	k value
1	A	–
2	B	0.413
3	A	–
4	A	–
5	A	–
6	A	–
7	B	0.550
8	B	0.951
9	A	–
10	B	0.697
11	A	–
12	B	0.689
13	B	0.296
14	A	–

Note: In the column for the model configuration, A corresponds to the model structure represented by Fig. 1(a) and Eq. (6a); B corresponds to the model structure represented by Fig. 1(b) and Eq. (6b). k value is needed only for configuration B.

While for the AoCo situation as described in Fig. 1b, a more complex model is used:

$$\Delta P_{all} = L_{asc}\cdot\frac{dQ_{asc}}{dt} + L_{dsc}\cdot\frac{dQ_{dsc}}{dt} + \frac{\rho(Q_{asc}-k(Q_{asc}-Q_{dsc}))^2}{2}\left(\frac{1}{A_{s1}^2}-\frac{1}{A_u^2}\right) + \frac{\rho Q_{dsc}^2}{2}\left(\frac{1}{A_{s2}^2}-\frac{1}{A_u^2}\right). \quad (6b)$$

where L_{asc} and L_{dsc} are the inertia of the blood flow in the ascending and descending aorta; Q_{asc} and Q_{dsc} the flow rates in the ascending and descending aorta; A_u the sectional area of the flow channels at the proximal side of the stenosis, A_s, A_{s1} and A_{s2} the sectional areas of the flow channel at the narrowest section of the different stenosis geometries, and k is a coefficient to describe the fractional flow into the vessels branches in the aortic arch, with the value in the range of 0–1. Detailed values for k in the individual patient cases are determined from the MRI measured flow change in the vessel branches and shown in Table 2.

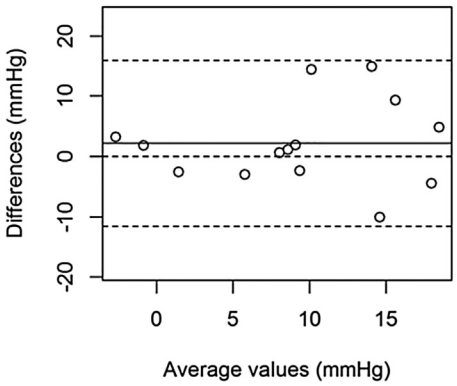

Fig. 3. Bland–Altman plot of the model prediction error for the pressure gradient in the 14 patient cases, based on the systolic peak-to-peak pressure values.

Parameterization of the model

MRI measurement directly provides the flow data in the ascending and descending aorta as well as in the vessel branches. The patient record has clearly stated the locations where the

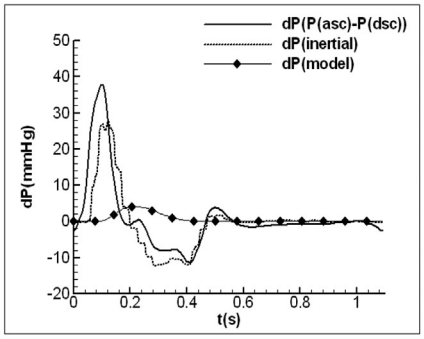

(a) Pressure gradient, neglecting the inertial effect

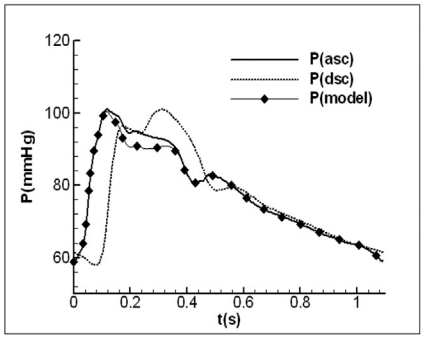

(b) Prediction of *dsc* pressure, neglecting the inertial effect

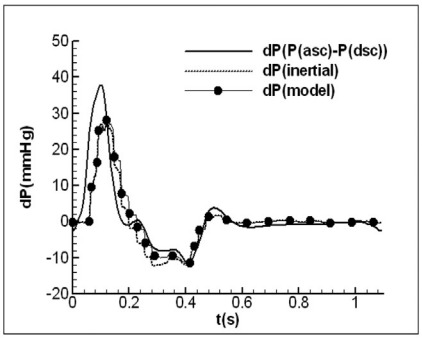

(c) Pressure gradient, considering the inertial effect

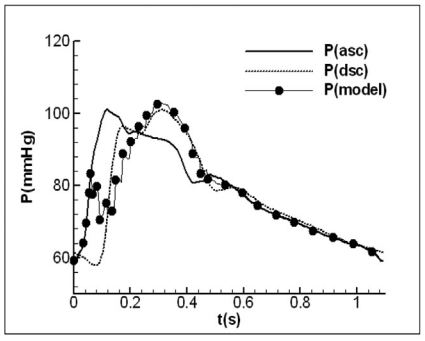

(d) Prediction of *dsc* pressure, considering the inertial effect

Fig. 2. Comparison of the model predicted pressure gradient and the pressure response in the descending aortic position (*dsc*) against the in vivo data, with and without considering the inertial effect, in the patient case 4. (*Note*: in (a) and (c), *dP*(*P*(*asc*) − *P*(*dsc*)) is the in vivo measured pressure gradient; in (b) and (d), *P*(*asc*) and *P*(*dsc*) are the catheter in vivo measured pressure response in the ascending (*asc*) and descending (*dsc*) aortic positions.)

pressure readings were taken during the catheterization procedure, which facilitates the calculation of the inertial effect of the blood flow. To accurately determine the sectional areas of the aorta in the stenosed section and the normal section, the MRI image sequence was imported into a free image analysis software called GIMIAS (http://www.gimias.org/, developed by CITB, University Pompeu Fabra, Barcelona, Spain), which enables the construction of the 3D vessel geometry from the 2D MRI image sequence. The diameter values at the mid-stenosis as well as for the normal vessel section were acquired using the measurement capability in GIAMIAS. The blood density is set as 1056 kg/m^3.

Results

The above introduced analysis procedure has been applied to study 14 patient cases of AoCo, and the model predicted pressure responses in the AoCo are compared against the catheter-measured in vivo data as illustrated in Figs. 2 and 3 and Tables 3–5.

Effect of inertial and frictional pressure drop in the patient cases

To evaluate the contribution of the inertial effect to the pressure gradient in the AoCo, Fig. 2 compares the pressure responses in

Table 3
Comparison of the model predicted and the catheter measured pressure gradients and the descending aortic pressure responses, in the 14 patient cases.

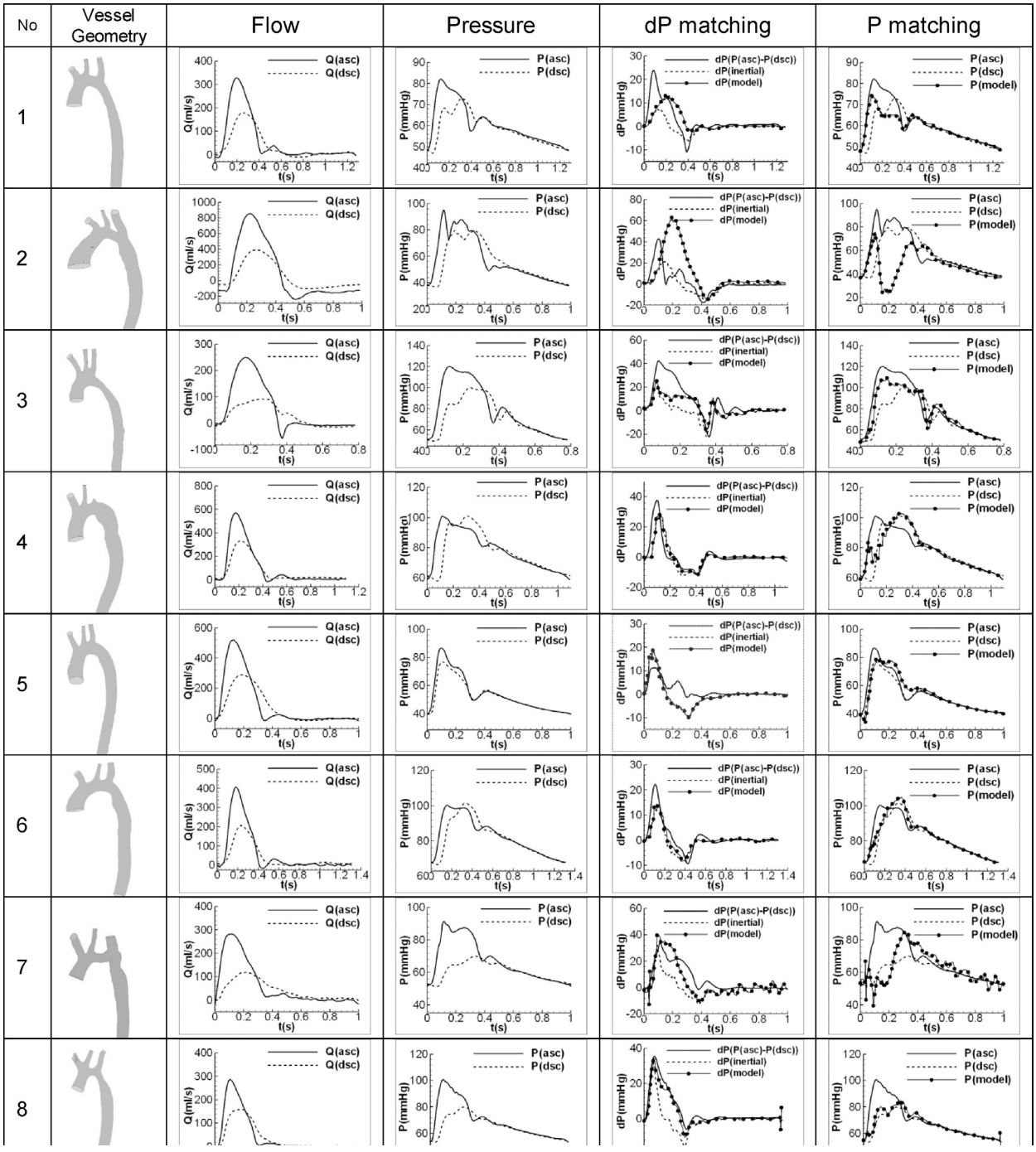

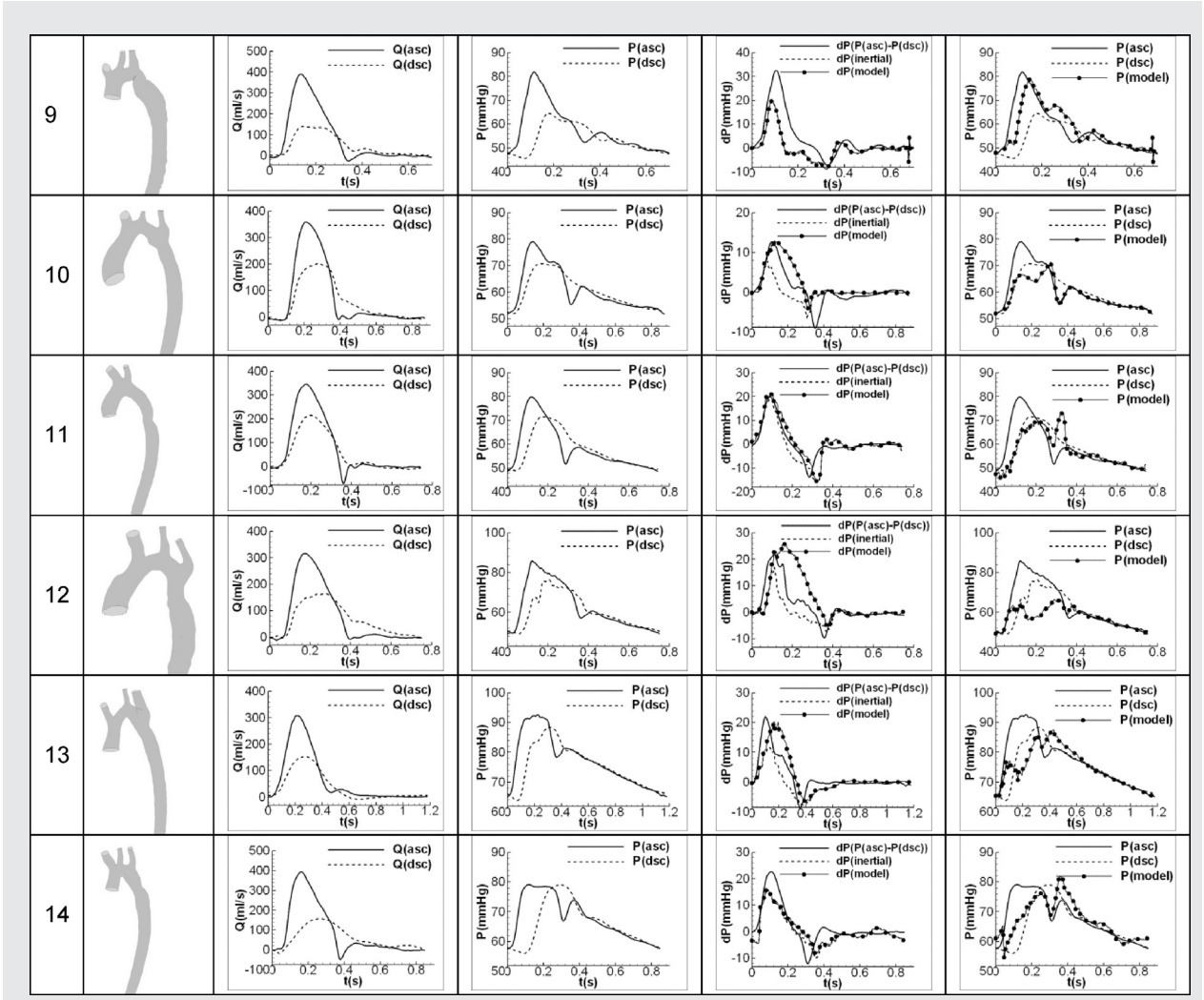

patient case 4 with/without considering the inertia effect. (a) and (c) of the figure show the changes of the inertial contribution [represented by the dQ/dt term in Eqs. (6a) and (6b)] and the model predicted overall pressure gradient ($dP_{model}(t)$, when the dQ/dt term is neglected or included) against the in vivo measured overall pressure gradient in the AoCo [$\Delta P_{all}(t) = P_{asc}(t) - P_{asc}(t)$] in a heart period. In (b) and (d) of the figure, the model-predicted overall pressure gradient is deducted from the in vivo measured ascending aortic pressure to produce the model-predicted descending aortic pressure [$\Delta P_{dsc,model}(t) = P_{asc}(t) - dP_{model}(t)$, when the dQ/dt term is neglected or included], and the predicted descending aortic pressure is compared with the in vivo measured descending aortic pressure $P_{dsc}(t)$ to demonstrate how the inertial effect influences the pressure gradient prediction. Comparison of (a) and (c) in Fig. 2 suggests that the inertial effect contributes to about 70% of the overall pressure gradient in early systole and about 90% in late systole in patient case 4. Overall, the inertial effect contributes significantly to the early and late systolic stages of the pressure gradient, while the frictional effect as represented by the stenosis models mainly influences the mid-systolic stage of the pressure gradient. By combing the inertial and frictional effects in the modeling, the predicted pressure gradient matches much better to the in vivo measured data than considering the frictional effect only. Contribution of the inertial effect in other patient cases is illustrated in the fifth column of Table 3, which also supports the above claim. The inertial effect is considered in all the following analysis.

Prediction and matching of pressure response in the patient cases

Table 3 presents the pressure gradient prediction in the AoCo and the P_{dsc} matching for the individual patient cases, and Table 4

Table 4
Statistics of the mean prediction error and the root mean square (RMS) prediction error, based on the cycle-averaged instantaneous pressure response, in the 14 patient cases (unit: mmHg).

Patient case	Model error	
	Mean	RMS
1	−0.56	4.94
2	8.19	22.07
3	−4.23	10.05
4	−0.34	5.44
5	−1.59	4.07
6	−1.06	2.94
7	−2.26	6.74
8	−1.58	2.65
9	−3.86	6.83
10	1.32	2.78
11	0.69	3.23
12	2.84	6.96
13	0.20	4.09
14	−1.39	4.19
Mean	0.26 ± 3.07	6.21 ± 5.01

Table 5
Statistics of invasively measured and non-invasively predicted descending aortic pressure and the pressure gradient, based on the systolic peak to peak value, in 14 patient cases (unit: mmHg).

Patient case	Invasively measured data			Model predicted data		Prediction error
	P_{asc}	P_{dsc}	ΔP	P_{dsc}	ΔP	ΔP
1	82.09	72.95	9.14	74.07	8.02	−1.12
2	95.57	79.84	15.73	75.4	20.17	4.44
3	120.12	99.86	20.26	109.17	10.95	−9.31
4	100.97	100.92	0.05	102.74	−1.77	−1.82
5	86.84	76.82	10.02	78.71	8.13	−1.89
6	100.36	101.42	−1.06	104.63	−4.27	−3.21
7	91.49	69.97	21.52	84.93	6.56	−14.96
8	100.78	79.92	20.86	84.73	16.05	−4.81
9	81.88	64.55	17.33	79.01	2.87	−14.46
10	79.1	70.77	8.33	71.4	7.7	−0.63
11	79.76	71.57	8.19	69.24	10.52	2.33
12	85.93	76.36	9.57	66.34	19.59	10.02
13	92.66	88.38	4.28	85.4	7.26	2.98
14	79.15	78.99	0.16	76.45	2.7	2.54
Mean						-2.14 ± 7.00

illustrates the statistics of the prediction error and RMS of the prediction error for the pressure gradient in the AoCo in each of the patient cases. It is observed that although in case 2 the mean prediction error for the pressure gradient is as high as 8.19 mmHg, and in cases 2 and 3 the RMS prediction error for the pressure gradient are 22.07 mmHg and 10.05 mmHg, which are much higher than the corresponding errors in other cases, the overall response matching has a case-averaged mean prediction error of only −0.26 mmHg and a case-averaged RMS prediction error of only 6.21 mmHg. Thus based on the criterion of cycle averaged instantaneous pressure gradient, the model prediction technique developed in this study produces consistent results with the in vivo measurement technique.

Evaluation of prediction error based on systolic peak to peak

In clinical practice, physicians often use the catheter-measured systolic peak to peak difference between P_{asc} and P_{dsc} ($\Delta P_{p-p} = P_{asc,sys,max} - P_{dsc,sys,max}$) to assist the AoCo diagnosis. Table 5 gives the statistics of the model predicted ΔP_{p-p} results against the catheter measured ΔP_{p-p} data in the 14 patient cases, in which the model prediction has a prediction error of -2.14 ± 7.00 mmHg. Fig. 3 shows the Bland–Altman plot of ΔP_{p-p} for the model predicted results and the in vivo measurement results, in which all the data points fall within the confidence interval, thus the model prediction technique developed in this study also produces consistent results with the in vivo measurement technique, based on the criterion of systolic peak to peak pressure gradient.

Discussion

Non-invasive estimation of the pressure gradient in AoCo has been an area of continuing interest in recent years, due to its potential applications in simplifying the clinical diagnosis. This study uses an MRI-based simple fluid mechanics model to predict the pressure gradient in AoCo, and compares the results with the catheter measured in vivo data in 14 AoCo patient cases. Comparison of the data based on the criteria of both the cycle-averaged instantaneous value and the systolic peak-to-peak value suggests that the current model prediction technique produces consistent results with that from the catheter in vivo measurement, thus verifies the accuracy and the reliability of the model prediction technique.

Based on the comparison of pressure response with and without considering the inertial effect, this study proves that the inertial effect makes a significant contribution to the overall pressure gradient in AoCo, given that the aortic flow is pulsatile and that the pressure gradient in AoCo is normally evaluated between vascular sections far upstream and downstream of the coarctation. Contribution of the inertial effect to the overall pressure gradient is predominantly in the systolic phase, when there is strong change rate in the flow. Since the inertial effect is governed by the density of the blood as well as the length and the sectional area of the vessel segment ($L = \rho \cdot \Delta x/A$), the longer the length of the vessel segment involved, the greater the inertial effect; or the smaller the sectional area of the vessel, the greater the inertial effect. This means that for other situations such as the blood flow in coronary atherosclerosis, the inertial effect should also be considered due to the pulsatile flow nature and the small vessel caliber.

A limitation of the current study is that the 14 cases of clinical data used do not make a significant data set. Thus the developed model-based prediction procedure needs to be further validated using larger numbers of patent data, before it can be accepted as a clinically workable technique.

Conclusion

In this research a non-invasive MRI-based modeling procedure is implemented to predict the pressure gradient in 14 cases of AoCo patient against the catheter-measured in vivo data. Results show that the inertial effect should be considered in modeling the pressure gradient in AoCo, due to the pulsatile aortic flow and the length of the vessel segment involved. Overall the MRI-based modeling procedure produces consistent results with that obtained from the catheter in vivo measurements, thus has the potential to be used in clinical practice as a non-invasive diagnosis tool in AoCo patients.

Funding

This research was supported by the European Commission's Seventh Framework Programme (FP7/2007-2013) under the grant agreement number 224495 (euHeart project).

Conflict of interest

The authors declare that there is no conflict of interest.

References

[1] Webb G. Treatment of coarctation and late complications in the adult. Semin Thorac Cardiovasc Surg 2005;17:139–42.

[2] Jurcut R, Daraban AM, Lorber A, Deleanu D, Amzulescu MS, Zara C, et al. Coarctation of the aorta in adults: what is the best treatment? Case report and literature review. J Med Life 2011;4:189–95.
[3] Kenny D, Hijazi ZM. Coarctation of the aorta: from fetal life to adulthood. Cardiol J 2011;18:487–95.
[4] Scheer B, Perel A, Pfeiffer UJ. Clinical review: complications and risk factors of peripheral arterial catheters used for haemodynamic monitoring in anaesthesia and intensive care medicine. Crit Care Lond Engl 2002;6:199–204.
[5] Tan RHH, Dart AJ, Dowling BA. Catheters: a review of the selection, utilisation and complications of catheters for peripheral venous access. Aust Vet J 2003;81:136–9.
[6] Brown AG, Shi Y, Marzo A, Staicu C, Valverde I, Beerbaum P, et al. Accuracy vs. computational time: translating aortic simulations to the clinic. J Biomech 2012;45:516–23.
[7] Keshavarz-Motamed Z, Rikhtegar Nezami F, Partida RA, Nakamura K, Staziaki PV, Ben-Assa E, et al. Elimination of transcoarctation pressure gradients has no impact on left ventricular function or aortic shear stress after intervention in patients with mild coarctation. JACC Cardiovasc Interv 2016;9:1953–65.
[8] Keshavarz-Motamed Z, Kadem L. 3D pulsatile flow in a curved tube with coexisting model of aortic stenosis and coarctation of the aorta. Med Eng Phys 2011;33:315–24.
[9] LaDisa JF, Alberto Figueroa C, Vignon-Clementel IE, Kim HJ, Xiao N, Ellwein LM, et al. Computational simulations for aortic coarctation: representative results from a sampling of patients. J Biomech Eng 2011;133:091008.
[10] Lien WW, Lee AH, Kono Y, Steinbach GC, Mattrey RF. Noninvasive estimation of the pressure gradient across stenoses using sonographic contrast: in vitro validation. J Ultrasound Med 2004;23:683–91.
[11] Hatle L, Angelsen BA, Tromsdal A. Non-invasive assessment of aortic stenosis by Doppler ultrasound. Br Heart J 1980;43:284–92.
[12] Hatle L, Brubakk A, Tromsdal A, Angelsen B. Noninvasive assessment of pressure drop in mitral stenosis by Doppler ultrasound. Br Heart J 1978;40:131–40.
[13] Dodds SR, Bourne NK, Chant AD. Effect of flow on the resistance of modelled femoral artery stenoses. Br J Surg 1996;83:957–61.
[14] Teirstein PS, Yock PG, Popp RL. The accuracy of Doppler ultrasound measurement of pressure gradients across irregular, dual, and tunnellike obstructions to blood flow. Circulation 1985;72:577–84.
[15] Marx GR, Allen HD. Accuracy and pitfalls of Doppler evaluation of the pressure gradient in aortic coarctation. J Am Coll Cardiol 1986;7:1379–85.
[16] Teien D, Karp K, Eriksson P. Non-invasive estimation of the mean pressure difference in aortic stenosis by Doppler ultrasound. Br Heart J 1986;56:450–4.
[17] Holen J, Simonsen S. Determination of pressure gradient in mitral stenosis with Doppler echocardiography. Br Heart J 1979;41:529–35.
[18] Seitz WS, Kashani IA. Non-invasive determination of the aortic valve area in stenosis: hydraulic orifice formula for application to echocardiography and correlation with catheterization. Eur Heart J 1983;4:31–40.
[19] Lima CO, Sahn DJ, Valdes-Cruz LM, Goldberg SJ, Barron JV, Allen HD, et al. Noninvasive prediction of transvalvular pressure gradient in patients with pulmonary stenosis by quantitative two-dimensional echocardiographic Doppler studies. Circulation 1983;67:866–71.
[20] Zhang Y, Nitter-Hauge S. Determination of the mean pressure gradient in aortic stenosis by Doppler echocardiography. Eur Heart J 1985;6:999–1005.
[21] Mustert BR, Williams DM, Prince MR. In vitro model of arterial stenosis: correlation of MR signal dephasing and trans-stenotic pressure gradients. Magn Reson Imaging 1998;16:301–10.
[22] Bock J, Frydrychowicz A, Lorenz R, Hirtler D, Barker AJ, Johnson KM, et al. In vivo noninvasive 4D pressure difference mapping in the human aorta: phantom comparison and application in healthy volunteers and patients. Magn Reson Med 2011;66:1079–88.
[23] Ebbers T, Wigström L, Bolger AF, Engvall J, Karlsson M. Estimation of relative cardiovascular pressures using time-resolved three-dimensional phase contrast MRI. Magn Reson Med 2001;45:872–9.
[24] Cantinotti M, Giordano R, Corsini I, Dani C, Scalese M, Murzi B, et al. Echocardiographic nomograms for upper abdominal aorta Doppler systolic wave values and systo-diastolic diameters variations in children. J Cardiol 2018;71:394–400.
[25] De Groote K, Devos D, Van Herck K, De Wolf D, Van der Straaten S, Rietzschel E, et al. Increased aortic stiffness in prepubertal girls with Turner syndrome. J Cardiol 2017;69:201–7.
[26] Muthurangu V, Taylor A, Andriantsimiavona R, Hegde S, Miquel ME, Tulloh R, et al. Novel method of quantifying pulmonary vascular resistance by use of simultaneous invasive pressure monitoring and phase-contrast magnetic resonance flow. Circulation 2004;110:826–34.
[27] Rhode KS, Hill DLG, Edwards PJ, Hipwell J, Rueckert D, Sanchez-Ortiz G, et al. Registration and tracking to integrate X-ray and MR images in an XMR facility. IEEE Trans Med Imaging 2003;22:1369–78.
[28] Hussain T, Lossnitzer D, Bellsham-Revell H, Valverde I, Beerbaum P, Razavi R, et al. Three-dimensional dual-phase whole-heart MR imaging: clinical implications for congenital heart disease. Radiology 2012;263:547–54.
[29] Weyman AE, Scherrer-Crosbie M. Aortic stenosis: physics and physiology – what do the numbers really mean? Rev Cardiovasc Med 2005;6:23–32.